LETTER Communicated by Anthony Burkitt

Mean, Variance, and Autocorrelation of Subthreshold Potential Fluctuations Driven by Filtered Conductance Shot Noise

Lars Wolff
wolff@mpipks-dresden.mpg.de
Benjamin Lindner
benji@mpipks-dresden.mpg.de
Max-Planck-Institut für Physik Komplexer Systeme, 01187 Dresden, Germany

We study the subthreshold voltage fluctuations of a conductance-based passive point neuron stimulated by filtered Poissonian shot noise. We give exact analytical expressions in terms of quadratures for the first two time-dependent moments and the autocorrelation function of the membrane voltage. We also derive simplified expressions for the moments in terms of elementary functions that hold true in the limit case of short filter time, small spike amplitude, and a single synaptic reversal potential. By means of these expressions, we show that for an ensemble of equilibrated conductances but sharp initial voltage (corresponding to a short voltage clamp at the initial time), the mean and the standard deviation can display nonmonotonic time courses. In particular, transient changes in the standard deviation disagree strongly with the predictions of the commonly used effective time constant approximation over a large parameter range. We also study the dependence of the correlation time of the voltage on the synaptic spike amplitude and the synaptic input rate. All results are confirmed by extensive stochastic simulations.

1 Introduction

Neurons are the basic unit of computation in our brain. The language in which they communicate information is the spike train, a sequence of small discharges of the voltage across their cell membrane of about 80 mV, a single one of which lasts less than a few ms (Koch, 1999). Because of the high connectivity in the neural networks of the cortex, a single neuron is subject to tens of thousands of such spike trains coming from other cells. Regardless of whether all of these presynaptic spike trains or only some of them represent information or just random fluctuations, the statistics of the synaptic input is in many cases well described by Poissonian shot noise, and, consequently, the resulting time course of the postsynaptic membrane potential and the resulting postsynaptic spike train appear to be stochastic too. Many researchers have modeled these fluctuations as a stochastic process

and have calculated their statistics (for reviews, see Holden, 1976; Ricciardi, 1977; Tuckwell, 1989; Gerstner & Kistler, 2002; Burkitt, 2006). In this work, we contribute to these efforts by an analysis of the time-dependent statistics of the postsynaptic voltage fluctuations without taking into account a postsynaptic spiking mechanism (passive membrane). Even in situations in which the neuron barely fires (e.g., for weak input noise or if an inhibitory current is applied), these subthreshold voltage fluctuations can still be of interest: their statistics are accessible by standard procedures and can provide useful information about synaptic properties (Rudolph, Piwkowska, Badoual, Bal, & Destexhe, 2004).

If the driving shot noise and synaptic filtering are properly taken into account, even the simplest model, a passive membrane, results in rather difficult stochastic equations. This model is addressed in this study. It was proposed in its original form by Stein (1965, 1967) and describes the fluctuating conductances of the membrane voltage dynamics by a linear filter equation with the spontaneous background shot noise as input. In slightly different versions, it has been studied in various papers. Until recently, only approximate results of varying range of validity were available. Two commonly used approaches are the diffusion approximation (see, e.g., Johannesma, 1968; Holden, 1976; Lánský & Lánská, 1987; Tuckwell, 1989; Burkitt, 2001; Lindner & Longtin, 2006) and the effective time-constant approximation (ECA), also called gaussian approximation (for reviews, see Richardson & Gerstner, 2005; Burkitt, 2006). A perturbation expansion approach going beyond the ECA for the asymptotic probability distribution and the steady-state moments of the voltage has been put forward by Richardson and Gerstner (2005).

In a recent publication (Wolff & Lindner, 2008), we proposed a method to calculate the exact time-dependent moments of the subthreshold voltage for arbitrary shot noise input. We used this method to calculate the time-dependent mean voltage for Poissonian shot noise input filtered by a first-order conductance dynamics. In this letter, we apply the same method for calculating the time-dependent standard deviation and the stationary correlation function of the subthreshold voltage. Furthermore, for the mean and the standard deviation, we give simple expressions in the limit of a fast synapse driven by a spike train with weak amplitudes.

We compare our exact results and our systematic approximation for two parameter sets (considering only one kind of synapse, respectively) with results of stochastic simulations and with the predictions of the common approximation, the ECA. Mean and standard deviation (SD) show extrema in the time course—features that are absent in the common approximation. Despite this qualitative failure of the ECA, we find that the time-dependent mean voltage and the steady-state SD value deviate only slightly from the ECA predictions. However, we also observe that the time-dependent standard deviation shows strong deviations for all parameter sets. Further, the exact correlation function shows a monotonic decay (as also predicted

by the ECA) with a time constant (correlation time), which differs for one of the parameter sets by a factor of three from the correlation time calculated in the ECA.

This letter is organized as follows. In section 2.1, the passive point neuron model is introduced. The concept of time-dependent moments is briefly explained in section 2.2, and the standard approximation to the problem (the ECA) is reviewed in section 2.3. The exact formulas for the time-dependent mean, the time-dependent standard deviation, and the stationary autocorrelation function are given in sections 2.4 to 2.6; here we also state simplified expressions for the time-dependent moments that are more accurate than the ECA. In section 3.1, we study the nonmonotonic behavior of the time-dependent moments. This is followed by an examination of the autocorrelation function and the correlation time in section 3.2. We briefly summarize and discuss our results in section 4.

2 Models and Methods

2.1 The Passive Point Neuron Model. Our study is based on the passive point neuron model as initially proposed by Stein (1965, 1967) and recently studied by Richardson (2004) and Richardson and Gerstner (2005). Its conductance dynamics is described by a linear filter equation with Poissonian shot noise input. This kind of linear filter has also been used by Brunel and Sergi (1998) and Richardson and Gerstner (2005) and showed reasonable agreement with experimental data (Destexhe & Mainen, 1994). A model with unfiltered Poissonian shot noise has been considered in Tuckwell (1979), and the case with unfiltered white gaussian noise has been treated in Hanson and Tuckwell (1983), Lánský and Lánská (1987), Burkitt (2001), and Richardson (2004).

The equations for the model considered here read:

$$C\frac{dV}{dt} = -(V - E_L)g_L - (V - E_e)g_e(t) - (V - E_i)g_i(t), \tag{2.1}$$

$$\tau_{\mathrm{e,i}}\frac{dg_{e,i}}{dt} = -g_{e,i} + c_{e,i}\tau_{\mathrm{e,i}}\sum_{\{t_{k_{e,i}}\}}\delta(t - t_{k_{e,i}}), \tag{2.2}$$

where e, i means either e or i, C is the membrane capacitance, and the leakage, excitatory, and inhibitory reversal potentials are denoted by E_L, E_e, and E_i, respectively. The respective conductances per area are abbreviated by g_L, $g_e(t)$, and $g_i(t)$. The synaptic filter is parameterized by the synaptic time constants $\tau_{\mathrm{e,i}}$ and the synaptic amplitudes $c_{e,i}$. The homogeneous Poissonian input process is characterized by the rate $r_{e,i}$.

A visualization of the dynamics is shown in Figure 1. In this example, the conductances are in a stationary state while the voltage was initially

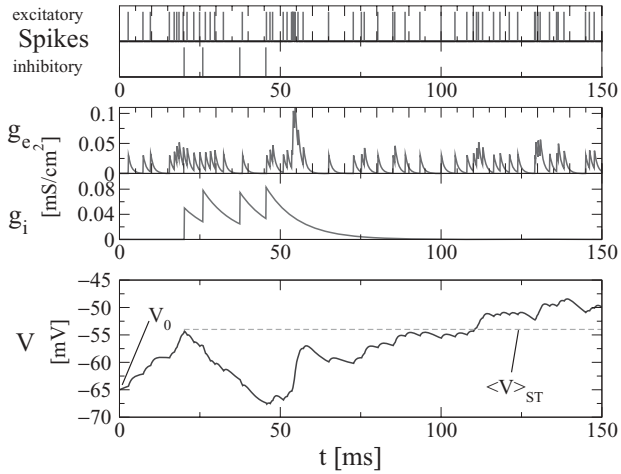

Figure 1: Visualization of the dynamics, obtained from the simulation of equations 2.1 and 2.2. Each time a spike arrives, the respective (inhibitory or excitatory) conductance makes a jump of size $c_{e,i}$ and then decays with time constant $\tau_{e,i}$ toward zero. The response of the voltage to a spike arrival is less regular, as the magnitude of the voltage change depends on the distance to the respective reversal potential. The discontinuous jump of the conductances is smoothed out due to the filtering, and the voltage is therefore a smoothly varying function of time. The parameters used for this example are $r_e = 400$ Hz, $r_i = 30$ Hz, $c_e = 0.3$ mS/cm^2, $c_i = 0.8$ mS/cm^2, $g_L = 0.3$ mS/cm^2, $\tau_e = 1$ ms, $\tau_i = 10$ ms, $C_m = 1\ \mu$F/cm^2, $E_e = -10$ mV, $E_i = -85$ mV, $E_L = -60$ mV, and $V_0 = -65$ mV.

clamped to a fixed value, $V_0 = -65$ mV. In the upper panel, the times of spike arrival are indicated by vertical lines for excitation and inhibition, respectively. The response of the respective conductances is shown in the middle panel. At the time of spike arrival, the conductance makes an instantaneous jump of magnitude $c_{e,i}$ and then decays toward zero until the next spike. The resulting voltage trajectory (bottom panel) shows a different behavior. Although the model contains a (discrete) shot noise input, the voltage is a continuously varying function of time. This is due to the finite filtering time. As the voltage depends on the fluctuating conductances in a multiplicative fashion, the magnitude of the voltage change caused by one spike is not fixed, but depends on the difference $V - E_{e,i}$. After a brief transient ($t \lesssim 10$ ms), the moments of the voltage approach constant values, as indicated by V_{ST} in Figure 1 (dashed line). The stationary SD for this example is $\sigma \approx 4.8$ mV.

Our study aims to characterize the effect of three nontrivial properties of the subthreshold dynamics equations, 2.1 and 2.2. The stimulus has shot noise character, is filtered by the first-order conductance dynamics, and

enters the voltage dynamics via conductance changes in a multiplicative fashion. All of these properties complicate the theoretical analysis and the calculation of the fluctuation's statistics; a gaussian continuous (instead of discontinuous), uncorrelated (instead of correlated), and additive (instead of voltage-dependent) noise would be more convenient in this respect. As we will show, the interplay of these nontrivial properties of the stochastic voltage dynamics strongly influences the features of the time-dependent voltage moments and can also change the autocorrelation function and, in particular, the correlation time, significantly.

For ease of notation, we will use a number of abbreviations in this letter:

$$v = V - E_L, \quad v_{e,i} = E_{e,i} - E_L, \quad v_0 = V_0 - E_L, \quad \beta = \frac{g_L}{C},$$
$$\varepsilon_{e,i} = \frac{c_{e,i}\tau_{\mathrm{e,i}}}{C}. \tag{2.3}$$

In our theory, regarding the relative amplitudes $\varepsilon_{e,i}$ as small permits a considerable simplification of the resulting formulas. We note that these amplitudes are nondimensional products of ratios

$$\varepsilon_{e,i} = \frac{c_{e,i}}{g_L}\frac{\tau_{\mathrm{e,i}}}{C/g_L} = \frac{c_{e,i}}{g_L}\frac{\tau_{\mathrm{e,i}}}{\tau_{\mathrm{mem}}}. \tag{2.4}$$

Here the first factor is the ratio of the increment of the conductance and the leak conductance of the unperturbed system. This factor will be small for an input spike train with small amplitude. The second factor is the ratio of conductance filter timescale and membrane time constant of the unperturbed system $\tau_{\mathrm{mem}} = C/g_L$. This ratio $\tau_{\mathrm{e,i}}/\tau_{\mathrm{mem}}$ is small for a "fast" synapse—a synaptic filter with a time constant smaller than that of the driven voltage dynamics. Simplifications of our formulas thus apply for neurons with fast synapses and small-amplitude shot noise input. Note that the firing rate of the input spike train does not enter the relative amplitudes $\varepsilon_{e,i}$, unlike small parameters used in other approximations (diffusion approximation or ECA).

2.2 Statistics of Interest: Time-Dependent Moments and Derived Measures. The first two time-dependent moments are given by $\langle V(t)\rangle$ and $\langle V(t)V(t')\rangle$, where the average is taken over an ensemble of time-dependent trajectories for which $V(t=0) = V_0$ and all conductances are equilibrated. This statistical ensemble corresponds to an ensemble of experiments where the voltage is initially briefly clamped to V_0 and it is assumed that this voltage clamp does not affect the synaptic conductances.

Two important statistical measures can be obtained from the first two time-dependent moments: the standard deviation $\sigma(t)$ and the stationary

autocorrelation function $c(\tau)$. The square of the time-dependent standard deviation is given by

$$\sigma^2(t) = \langle V^2(t)\rangle - \langle V(t)\rangle^2, \tag{2.5}$$

and the autocorrelation function reads

$$c(\tau) = \lim_{t\to\infty}(\langle V(t)V(t+\tau)\rangle - \langle V(t)\rangle^2). \tag{2.6}$$

Nonoscillating correlation functions can be characterized by the correlation time:

$$\tau_c = \frac{1}{c(0)}\int_0^\infty d\tau\ c(\tau). \tag{2.7}$$

For purely exponential autocorrelation functions, τ_c is equal to the decay time constant.

To obtain a moment from experiments or simulations, the first step is to record N time-dependent voltage trajectories, where N is a large number. The trajectories are obtained by imposing an initial condition to the voltage (e.g., by clamping the cell to the voltage V_0), releasing the constraint and recording the voltage until the dynamics is in a steady state ($\approx$50 ms). An important assumption for the methods used to derive the results of this letter is that the conductances are equilibrated. From the moments of this ensemble of time-dependent voltage trajectories, one can obtain estimates for the time-dependent moments of the subthreshold voltage fluctuations. This procedure is illustrated in Figure 2 for the time-dependent mean value and the time-dependent standard deviation.

Stationary quantities (such as the autocorrelation function, which is also calculated in this letter), can be extracted much more easily, from voltage recordings: one needs only one long stationary voltage trace to extract the correlation function with a moving-window algorithm.

2.3 Approximate Expressions for Mean, Standard Deviation, and Correlation Function Using the Effective Time Constant Approximation. The passive point neuron model consists of three stochastic differential equations with multiplicative noise in the voltage and shot noise input to the conductances. The solution of the equations is rather challenging, and in many cases, approximations have been used.

The following standard approximation is widely used in the case of Poissonian input spike trains (see Burkitt, 2006; Richardson & Gerstner, 2005). For a high input rate and a small impact of a single spike on the conductances (represented by c_e and c_i in this model), the Poissonian input noise in equation 2.2 can be replaced by a gaussian white noise process. Moreover, the multiplicative contributions to the dynamics can be neglected.

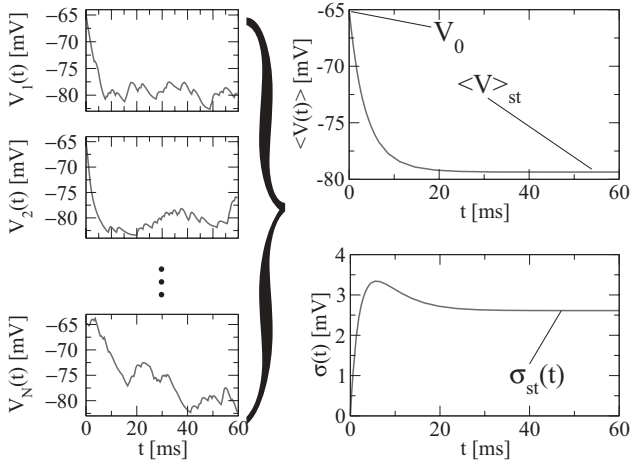

Figure 2: Estimating the time-dependent mean value and standard deviation from voltage traces. After recording N time-dependent voltage traces with initial voltage $V(0) = V_0$ (left panel), one has to take the arithmetic mean of the N traces to obtain an estimate for the time-dependent mean value of the neuron (upper right panel). The asymptotic (stationary) mean voltage $\langle V \rangle_{st}$ is indicated. To obtain an estimate of the variance, one has to subtract the squared time-dependent mean value from the arithmetic mean of the squared traces. The standard deviation, which is the square root of the variance, is shown in the lower right panel.

This leads to the following simplified equations:

$$C\frac{dV}{dt} = -(V - E_0)g_0 - (E_e - E_0)g_{eF}(t) - (E_i - E_0)g_{iF}(t), \tag{2.8}$$

$$\tau_{\mathrm{e,i}}\frac{dg_{e,i;F}}{dt} = -g_{e,i;F} + \sqrt{2\tau_{\mathrm{e,i}}\sigma_{e,i}^2}\xi_{e,i}(t). \tag{2.9}$$

Here, E_0 and g_0 are the new effective leakage reversal potential and leakage conductance, respectively. They are given by

$$g_0 = g_L + g_{e0} + g_{i0}, \tag{2.10}$$

$$E_0 = \frac{1}{g_0}(g_L E_L + g_{e0}E_e + g_{i0}E_i + I_{\mathrm{app}}), \tag{2.11}$$

with $g_{e,i;0} = c_{e,i}\tau_{\mathrm{e,i}}r_{e,i}$, $\sigma_{e,i} = c_{e,i}\sqrt{\tau_{\mathrm{e,i}}r_{e,i}/2}$. The gaussian white noise process $\xi_{e,i}(t)$ is characterized by $\langle\xi\rangle = 0$, and $\langle\xi(t)\xi(t+\tau)\rangle = \delta(\tau)$.

This is the so-called effective time constant approximation (ECA) (also called a gaussian approximation) because the equations resemble a passive point neuron with current noise, where the membrane time constant C/g_L is replaced by the effective time constant $\tau_0 = C/g_0$. From equations 2.8 and 2.9, one can easily obtain all moments. We will compare the exact results obtained in the following section to the predictions of the ECA. For this purpose, we explicitly give the expressions for the time-dependent mean and variance as well as the autocorrelation function as predicted by the ECA:

$$\begin{aligned}\langle V(t)\rangle_{ECA} &= (V_0 - E_0)e^{-t/\tau_0} + E_0,\\ &= v_0 e^{-t/\tau_0} + (1 - e^{-t/\tau_0})(r_e\varepsilon_e v_e + r_i\varepsilon_i v_i)\tau_0 + E_L, \qquad (2.12)\\ \sigma^2(t)_{ECA} &= \left(\frac{E_e - E_0}{g_0}\right)^2 \sigma_e^2 \frac{\tau_e^2}{\tau_e^2 - \tau_0^2}\left(1 - \frac{\tau_0}{\tau_e} + e^{-2\frac{t}{\tau_0}}\left(1 + \frac{\tau_0}{\tau_e}\right)\right.\\ &\quad \left. - 2e^{-(\frac{1}{\tau_0}+\frac{1}{\tau_e})t}\right) + \left(\frac{E_i - E_0}{g_0}\right)^2 \sigma_i^2 \frac{\tau_i^2}{\tau_i^2 - \tau_0^2}\\ &\quad \times \left(1 - \frac{\tau_0}{\tau_i} + e^{-2\frac{t}{\tau_0}}\left(1 + \frac{\tau_0}{\tau_i}\right) - 2e^{-(\frac{1}{\tau_0}+\frac{1}{\tau_i})t}\right)\\ &= ((1 - r_e\varepsilon_e\tau_0)v_e - r_i\varepsilon_i\tau_0 v_i)^2 \frac{r_e}{2}\varepsilon_e^2\tau_0^2\frac{\tau_e}{\tau_e^2 - \tau_0^2}\\ &\quad \times \left(1 - \frac{\tau_0}{\tau_e} + e^{-2\frac{t}{\tau_0}}\left(1 + \frac{\tau_0}{\tau_e}\right) - 2e^{-(\frac{1}{\tau_0}+\frac{1}{\tau_e})t}\right)\\ &\quad + ((1 - r_i\varepsilon_i\tau_0)v_i - r_e\varepsilon_e\tau_0 v_e)^2 \frac{r_i}{2}\varepsilon_i^2\tau_0^2\frac{\tau_i}{\tau_i^2 - \tau_0^2}\\ &\quad \times \left(1 - \frac{\tau_0}{\tau_i} + e^{-2\frac{t}{\tau_0}}\left(1 + \frac{\tau_0}{\tau_i}\right) - 2e^{-(\frac{1}{\tau_0}+\frac{1}{\tau_i})t}\right), \qquad (2.13)\end{aligned}$$

and

$$\begin{aligned}c(\tau)_{ECA} &= \left(\frac{E_e - E_0}{g_0}\right)^2 \sigma_e^2 \frac{\tau_e^2}{\tau_e^2 - \tau_0^2}\left(e^{-\frac{\tau}{\tau_e}} - \frac{\tau_0}{\tau_e}e^{-\frac{\tau}{\tau_0}}\right)\\ &\quad + \left(\frac{E_i - E_0}{g_0}\right)^2 \sigma_i^2 \frac{\tau_i^2}{\tau_i^2 - \tau_0^2}\left(e^{-\frac{\tau}{\tau_i}} - \frac{\tau_0}{\tau_i}e^{-\frac{\tau}{\tau_0}}\right)\\ &= ((1 - r_e\varepsilon_e\tau_0)v_e - r_i\varepsilon_i\tau_0 v_i)^2 \frac{r_e}{2}\varepsilon_e^2\tau_0^2\frac{\tau_e}{\tau_e^2 - \tau_0^2}\left(e^{-\frac{\tau}{\tau_e}} - \frac{\tau_0}{\tau_e}e^{-\frac{\tau}{\tau_0}}\right)\\ &\quad + ((1 - r_i\varepsilon_i\tau_0)v_i - r_e\varepsilon_e\tau_0 v_e)^2 \frac{r_i}{2}\varepsilon_i^2\tau_0^2\frac{\tau_i}{\tau_i^2 - \tau_0^2}\left(e^{-\frac{\tau}{\tau_i}} - \frac{\tau_0}{\tau_i}e^{-\frac{\tau}{\tau_0}}\right). \qquad (2.14)\end{aligned}$$

For pure inhibition or excitation, all of these functions are monotonic in t, and the correlation time for equation 2.14 takes a very simple form:

$$\tau_{c,ECA} = \tau_0 + \tau_{\mathrm{e,i}}. \tag{2.15}$$

For both excitation and inhibition present, the SD can show an overshoot. Note that the time-dependent standard deviation, equation 2.13, is completely independent of the initial voltage.

Finally, we state an approximate result by Richardson and Gerstner (2005) for the steady-state mean value, which goes beyond the ECA:

$$\begin{aligned}\langle V\rangle_\infty^{RG} &= E_0 - \left(\frac{\sigma_e^2}{g_0^2}(E_e - E_0)\frac{\tau_e}{\tau_e+\tau_0} + \frac{\sigma_i^2}{g_0^2}(E_i - E_0)\frac{\tau_i}{\tau_i+\tau_0}\right) \\ &\quad + \mathcal{O}\left(\left(\frac{\sigma_{e,i}}{g_0}\right)^3\right) \\ &= E_L + \varepsilon_e r_e \tau_0 v_e + \varepsilon_i r_i \tau_0 v_i - \left(\frac{r}{2(\tau_e+\tau_0)}\varepsilon_e^2\tau_0^2((1 - r_e\varepsilon_e\tau_0)v_e\right. \\ &\quad \left. - r_i\varepsilon_i\tau_0 v_i) + \frac{r_i}{2(\tau_i+\tau_0)}\varepsilon_i^2\tau_0^2\left((1 - r_i\varepsilon_i\tau_0)v_i - r_e\varepsilon_e\tau_0 v_e\right)\right) \\ &\quad + \mathcal{O}\left(\left(\frac{r_{e,i}\varepsilon_{e,i}\tau_0}{\tau}\right)^3\right).\end{aligned} \tag{2.16}$$

In the derivation of this result, it was assumed that the following parameters are small:

$$\delta_{e,i}^{RG} = \frac{\sigma_{e,i}}{g_0} = \frac{c_{e,i}\sqrt{\tau_{\mathrm{e,i}} r_{e,i}/2}}{g_L + c_i\tau_i r_i + c_e\tau_e r_e} \ll 1. \tag{2.17}$$

According to Richardson and Gerstner (2005), there is within the same approximation no correction to the steady-state variance as predicted by the ECA.

2.4 Exact Formula for the Mean. Using the methods introduced by Wolff and Lindner (2008), one obtains for the time-dependent mean value for Poissonian shot-noise input,

$$\begin{aligned}\big\langle v(t)\big\rangle &= v_0 \exp\left[-\beta t + f_e(t) + f_i(t)\right] \\ &\quad - v_e\int_0^t ds \exp\left[-\beta s + f_e(s) + f_i(s)\right]\frac{df_e(s)}{ds} \\ &\quad - v_i\int_0^t ds \exp\left[-\beta s + f_e(s) + f_i(s)\right]\frac{df_i(s)}{ds}.\end{aligned} \tag{2.18}$$

The functions $f_{e,i}(t)$ are given in appendix A. Due to the complicated form of these functions, the integrals appearing in equation 2.18 have to be solved numerically.

The resulting formulas can be simplified for weak relative amplitudes $\varepsilon_{e,i} \ll 1$ where the exponential occurring in the moments can be approximated as follows (Wolff, 2007):

$$\exp[f(s)] \approx e^{-r\varepsilon s}\left(1 + \frac{1}{2}r\tau\varepsilon^2\left(\frac{s}{\tau} + \left(e^{-s/\tau} - 1\right)\right)\right). \tag{2.19}$$

Here we have omitted the respective index e or i for rates, amplitude, and time constant. When the expansion is inserted into the exact formulas, all integrals can be performed analytically. Here we restrict ourselves to the case of only one synaptic reversal potential (either pure excitation or pure inhibition). With the abbreviation $\tau_{\mathrm{e,i}} = \tau$, the expression reads as follows:

$$\left\langle v(t)\right\rangle \approx \langle V\rangle_\infty^{RG} - E_L + c_{\langle v\rangle,1}(t)e^{-t/\tau_0} + c_{\langle v\rangle,2}e^{-(1/\tau_0+1/\tau)t}, \tag{2.20}$$

where $\langle V\rangle_\infty^{RG}$ is the steady-state value calculated by Richardson and Gerstner (2005), and $c_{\langle v\rangle,1}(t)$ and $c_{\langle v\rangle,2}$ are a linear function of t and a constant, respectively, which are given in section B.1. Note that we use an asymptotic expansion for the integrands of equation 2.18. This implies that the full integral is not an asymptotic expansion anymore; however, it is still an asymptotic approximation. In other words, although we expanded the integrand to a certain power in ε, we cannot say about the whole integral that it is of a particular order in ε. In the rest of this letter, when we speak of the expansion to a certain order, we always mean that we expanded the integrand and inserted it into equation 2.18.

The approximation equation, 2.21, includes corrections up to order ε^2 and is expected to work for small ε at any time t; in linear order in ε, it corresponds to the ECA. Note that although we have used a slightly different expansion parameter (ε given in equation 2.3 instead of δ^{RG} given in equation 2.17), the steady-state value of the voltage is the same as the one calculated by Richardson and Gerstner (2005).

2.5 Exact Formula for the Standard Deviation. With the methods by Wolff and Lindner (2008), the second time-dependent moment $\langle v^2(t)\rangle$ yields (for details, see also Wolff, 2007)

$$\begin{aligned}\langle v^2(t)\rangle = {} & v_0^2 e^{-2\beta t}e^{f_{e>}(t,t)}e^{f_{i>}(t,t)} - 2v_0v_e\int_0^t ds' e^{-\beta(t+s')}e^{f_{i>}(t,s')}\frac{d}{ds'}e^{f_{e>}(t,s')} \\ & - 2v_0v_i\int_0^t ds' e^{-\beta(t+s')}e^{f_{e>}(t,s')}\frac{d}{ds'}e^{f_{i>}(t,s')}\end{aligned}$$

$$
\begin{aligned}
&+ 2v_e^2 \int_0^t ds \int_0^s ds' e^{-\beta(s+s')} e^{f_{i>}(s,s')} \frac{d^2}{dsds'} e^{f_{e>}(s,s')} \\
&+ 2v_i^2 \int_0^t ds \int_0^s ds' e^{-\beta(s+s')} e^{f_{e>}(s,s')} \frac{d^2}{dsds'} e^{f_{i>}(s,s')} \\
&+ 4v_e v_i \int_0^t ds \int_0^s ds' e^{-\beta(s+s')} \left(\frac{d}{ds} e^{f_{e>}(s,s')} \right) \left(\frac{d}{ds'} e^{f_{i>}(s,s')} \right).
\end{aligned}
\tag{2.21}
$$

The functions $f_{e,i>}(s, s')$ are given in appendix A. Again, the complicated structure of these functions precludes the analytical evaluation of the integrals in equation 2.21. A numerical evaluation of the integrals is, however, straightforward and, with the evaluation of equation 2.18, provides via equation 2.5 the exact standard deviation.

Furthermore, as in the case of the mean, we can also calculate an approximation that holds true for small relative amplitudes $\varepsilon_{e,i}$ using approximations for the exponential functions appearing in the above formula (see section B.2). Again, all resulting integrals can be carried out explicitly; the resulting expression for the time-dependent variance (and for only excitation or inhibition present) reads

$$
\begin{aligned}
\langle v^2(t) \rangle \approx\ & c_{\langle v^2 \rangle,1}(t) e^{-2t/\tau_0} + c_{\langle v^2 \rangle,2}(t) e^{-t/\tau_0} + c_{\langle v^2 \rangle,3} e^{-(2/\tau_0 + 1/\tau)t} \\
& + c_{\langle v^2 \rangle,4} e^{-(1/\tau_0 + 1/\tau)t} + c_{\langle v^2 \rangle,5},
\end{aligned}
\tag{2.22}
$$

where the first two coefficients are linear in t and the last three are constants; all are given in section B.2 and $\tau = \tau_{e,i}$. In contrast to the ECA, this result can also predict a nonmonotonic behavior of the variance (see below). Note that the lowest order (ε) of this systematic approximation does not correspond to the ECA (in contrast to the mean value). This is due to the nonlinear character of the variance, as explained in the following: The ECA roughly corresponds to a lowest-order expansion of the stochastic process $V(t) = v(t) + E_L$. The systematic approximation proposed in this section, in contrast, is an expansion of the moments of the stochastic process $v(t)$. Thus, one can reckon the first (linear) moment of the ECA process to agree with the leading order of the systematic expansion of the mean value. For the higher moments, however, one might expect discrepancies between the two approaches. In particular, the variance of the ECA approximation (which is quadratic in the approximated process and thereby higher order) will be different to the leading-order expansion of the exact second moment.

We emphasize that our systematic approximation is a rigorous procedure. Moreover, by calculating the next term of the expansion, one can also obtain a measure for the error.

2.6 Exact Formula for the Autocorrelation Function. According to Wolff and Lindner (2008) and Wolff (2007), the asymptotic second moment for Poissonian shot noise can be calculated by

$$\begin{aligned}
&\lim_{t\to\infty}\left\langle v(t)v(t+\tau)\right\rangle \\
&= 2\int_0^\infty ds\int_0^s ds' e^{-\beta(\tau+s+s')}\left\{(v_e^2 e^{f_{i>}^+(s,s',\tau)}\frac{d^2}{dsds'}e^{f_{e>}^+(s,s',\tau)}\right. \\
&+ v_i^2 e^{f_{e>}^+(s,s',\tau)}\frac{d^2}{dsds'}e^{f_{i>}^+(s,s',\tau)} + v_e v_i\left(\frac{d}{ds}e^{f_{i>}^+(s,s',\tau)}\right)\left(\frac{d}{ds'}e^{f_{e>}^+(s,s',\tau)}\right) \\
&\left.+ v_e v_i\left(\frac{d}{ds}e^{f_{e>}^+(s,s',\tau)}\right)\left(\frac{d}{ds'}e^{f_{i>}^+(s,s',\tau)}\right)\right\} \\
&+ \int_0^\infty ds\int_{-\tau}^0 ds' e^{-\beta(\tau+s+s')}\left\{v_e^2 e^{f_{i>}^-(s,s',\tau)}\frac{d^2}{dsds'}e^{f_{e>}^-(s,s',\tau)}\right. \\
&+ v_i^2 e^{f_{e>}^-(s,s',\tau)}\frac{d^2}{dsds'}e^{f_{i>}^-(s,s',\tau)} + v_e v_i\left(\frac{d}{ds}e^{f_{i>}^-(s,s',\tau)}\right)\left(\frac{d}{ds'}e^{f_{e>}^-(s,s',\tau)}\right) \\
&\left.+ v_e v_i\left(\frac{d}{ds}e^{f_{e>}^-(s,s',\tau)}\right)\left(\frac{d}{ds'}e^{f_{i>}^-(s,s',\tau)}\right)\right\}. \qquad (2.23)
\end{aligned}$$

The functions $f_{e,i>}^{\pm}$ are given in appendix A. Also in this case, the integrals in equation 2.23 have to be evaluated numerically.

The exact autocorrelation function can be calculated using equations 2.6, 2.18, and 2.23.

2.7 Stochastic Simulation Algorithm. To generate the Poissonian time series for the input spike train, a random number between 0 and 1 was drawn, using the function *rand* of the programming language C. If this number was smaller than $r_{e,i}$ times the integration time step dt, a spike was generated. One time step after the occurrence of a spike, the respective conductance was increased by $c_{e,i}$. Using these conductances, a discretized version of equation 2.1 was integrated using a simple Euler integration scheme.

To obtain mean and variance, at each time step, $V(t)$ and $V^2(t)$ were recorded, and the arithmetic mean was taken over N independent trajectories. The autocorrelation function was obtained by the following procedure. After a certain waiting time to ensure that the system relaxed to a stationary state, the asymptotic time-dependent trajectory $V_\infty(j \times dt)$ was recorded, and the quantity $V_\infty(j \times dt) - \langle V_\infty\rangle$ was Fourier transformed. The square of the absolute value of the Fourier transform was averaged over many independent trajectories to obtain the power spectrum (see, e.g., Gardiner, 1985, equation 1.4.34). According to the Wiener-Khinchin theorem (see, e.g.,

Table 1: Standard Parameter Set 1.

Parameter	Standard Set 1
r_e	800 Hz
τ_e	3 ms
c_e	$0.03\,\frac{\mathrm{mS}}{\mathrm{cm}^2}$
E_e	-30 mV
E_L	-90 mV
C	$1\,\frac{\mu\mathrm{F}}{\mathrm{cm}^2}$
g_L	$0.05\,\frac{\mathrm{mS}}{\mathrm{cm}^2}$
τ_{mem}	20 ms

Note: Here the relative amplitude $\varepsilon_e = 0.09$ is much smaller than one.

Table 2: Standard Parameter Set 2.

Parameter	Standard Set 2
r_i	20 Hz
τ_i	10 ms
c_i	$2\,\frac{\mathrm{mS}}{\mathrm{cm}^2}$
E_i	-90 mV
E_L	-65 mV
C	$1\,\frac{\mu\mathrm{F}}{\mathrm{cm}^2}$
g_L	$0.05\,\frac{\mathrm{mS}}{\mathrm{cm}^2}$
τ_{mem}	20 ms

Note: In this case, the relative amplitude $\varepsilon_i = 20$ is larger than one.

Gardiner, 1985, equation 1.4.39), the inverse Fourier transform of the power spectrum yields the autocorrelation function.

3 Results

In this section we compare our exact results for mean and standard deviation to stochastic simulations, the ECA, and our weak-amplitude approximations equations 2.20 and 2.22. We also inspect the correlation function and the correlation time that can be derived from it.

In the following, two standard parameter sets are used to which we refer in most of our numerical examples (see Tables 1 and 2). For both sets, only one synaptic input is present. Standard set 1 describes a neuron with many but weak (excitatory) synaptic connections. The high rate and the weak

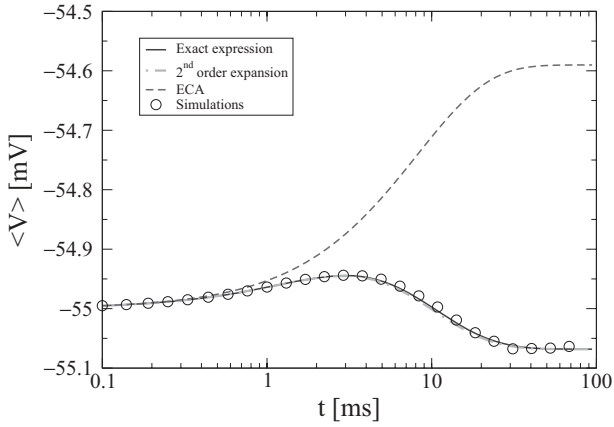

Figure 3: Exact mean voltage (solid line), systematic approximation (dash-dot line) and ECA expression (dashed line) compared to simulation results (circles). The exact mean value has a maximum at $t \approx 3$ ms, which is very well reproduced by the systematic approximation. The ECA fails to predict nonmonotonic behavior. The parameters are taken from standard set 1 (see Table 1) and the initial voltage is -55 mV.

noise indicate that the ECA should be a good approximation for this set. Standard set 2 represents a neuron with few but strong (inhibitory) synaptic connections. Due to the low rate and the strong noise, one expects that the ECA description will fail for this set.

3.1 Nonmonotonic Behavior of the Transient Moments. We have shown (Wolff & Lindner, 2008) that the time-dependent mean value exhibits an extremum if the initial voltage is chosen in an appropriate way. The parameter set in Table 1 is similar to one of the sets used in Wolff and Lindner. The mean value for these parameters is presented in Figure 3. The exact mean value shows a maximum versus time. This is also very well reproduced by the systematic approximation presented in the last section. In contrast, the ECA is not able to reproduce this nonmonotonic behavior. Also, the asymptotic value of the systematic approximation is in better agreement with the exact value than the ECA. Note, however, that the quantitative deviations of the ECA for this set are very small as compared to the SD (see Figure 5). Therefore, if one is interested in the mean value, using the ECA is in most cases completely justified for this set.

An example for the standard set 2 (see Table 2) is given in Figure 4, where we plot the exact mean, the prediction of the ECA, and the simulation results versus time. The exact curve and the ECA prediction agree for $t < 0.2$ ms. For longer times, the ECA prediction decays exponentially, whereas the exact curve reaches a minimum (in contrast to the excitatory example,

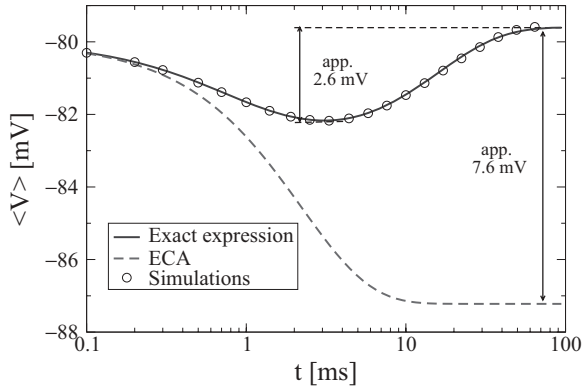

Figure 4: Example for a nonmonotonic mean. The exact mean value (solid curve) has a minimum at $t \approx 3$ ms, whereas the ECA prediction shows a purely exponential time curse. The parameters are taken from standard set 2 (see Table 2), and the initial voltage is -80 mV. The simulations are averaged over 10^5 trajectories.

where a maximum was observed) at $t \approx 3$ ms and then increases until it attains a stationary value. The magnitude of the extremum for this example is approximately 2.6 mV. The systematic approximation is not shown for this set, as the requirement of a small relative amplitude ε is not met.

To obtain a nonmonotonic mean value, the initial value has to lie within a narrow range, the width of which is determined by the other parameters of the system (Wolff & Lindner, 2008). However, it could be proven that there always exist initial values that lead to a nonmonotonic behavior (Wolff & Lindner, 2008), although the latter is not necessarily typical.

A nonmonotonic behavior of the SD as a function of time is much more typical. Figure 5a shows the SD for different initial voltages, most of which lead to a maximum attained between 7 and 10 ms. In Figure 5b, the standard deviation for the initial value of -80 mV is compared to the approximations and to simulation results. The ECA prediction does not change at all with the initial voltage (see equation 2.13). Only for moderate initial voltages is the SD monotonic and in agreement with the ECA prediction (compare the lowest curve in Figure 5a to the ECA curve in Figure 5b). The systematic approximation, however, fits the nonmonotonic behavior of the standard deviation very well. The fact that we found the exact expressions for the moments is supported by the excellent agreement of our theory to numerical simulation results of the full model.

An even more interesting behavior can be observed for the standard set 2, which has only an inhibitory conductance. Figure 6 shows the exact SD for this set for different initial values. In contrast to the excitatory example, one

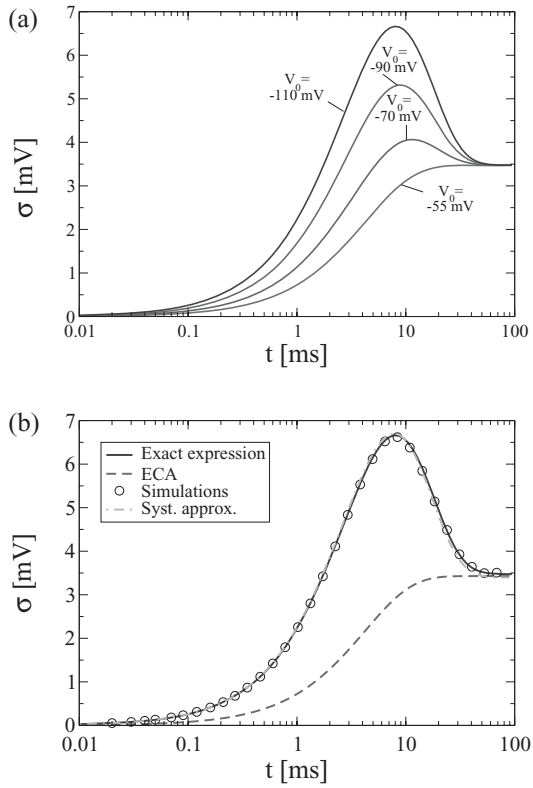

Figure 5: (a) The exact standard deviation for different initial voltages for standard set 1 (see Table 1). For moderate initial voltages, $V_0 \approx \langle V \rangle_{ST}$ (lowest curve), the time course is monotonic. If the initial voltage is decreased, a maximum develops. The maximum becomes more pronounced the lower the initial voltage is. (b) The curve for the lowest initial value is compared to results of stochastic simulations (circles), the ECA (dashed line), and the systematic approximation (dash-dot line).

observes maxima for initial voltages larger than the steady-state mean value (in this case, $\langle V \rangle_{ST} \approx -80$ mV). For initial voltages between the steady-state mean voltage and the inhibitory reversal potential ($E_i = -90$ mV for this example), the SD is monotonic. Interestingly, for initial voltages smaller than E_i, one again observes a nonmonotonic time course with a minimum and a maximum. The extrema become more pronounced as the difference of the initial voltage to the synaptic reversal potential grows.

We conclude that if the parameters meet the requirements of section 2.3 and one is interested only in the stationary mean and SD, using the ECA

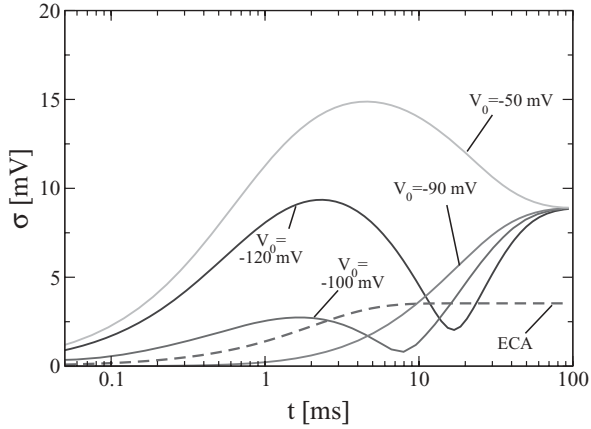

Figure 6: The exact standard deviation for different initial voltages for standard set 2. As in Figure 5, a monotonic time course can be observed for moderate initial voltages. In this case, however, for large initial voltages (the reference point is always the steady-state mean voltage), the curve shows a maximum, and for low initial voltages $V_0 < E_i$, one can see a minimum and a maximum.

expression is justified. However, even in cells where deviations between the predictions for the stationary quantities of the ECA and the exact expressions are small, transient differences in the SD can be large. These may be important for the spiking statistics in the presence of voltage-gated ion channels (i.e., a spike-generating mechanism).

3.2 The Autocorrelation Function. As the autocorrelation function is calculated from the stationary moments, there is no dependence on the initial voltage. The nontrivial dependence on the initial voltage was one major effect of the multiplicative dynamics and the shot noise input and revealed interesting effects such as a nonmonotonic time course. Nevertheless, there is a difference in the timescale between the full multiplicative dynamics and the additive dynamics with a gaussian input noise (represented by the ECA). As a measure for the typical timescale of the correlation function, we use the correlation time as introduced in equation 2.7.

Figure 7 shows the exact autocorrelation function, the ECA prediction, and simulation results for standard set 1. The exact curve and the simulations agree very well, and the ECA prediction is in reasonable agreement. The correlation times for this example are $\tau_{c,ex} = 11.4$ ms and $\tau_{c,ECA} = 11.2$ ms.

For standard set 2, more drastic deviations can be observed, as can be seen in Figure 8. We note that the deviations at small time lags are related to the difference between the true and approximate stationary standard

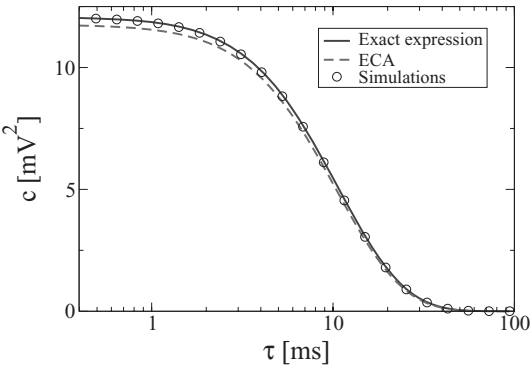

Figure 7: Comparison of the exact autocorrelation function, the ECA prediction, and simulation results for standard set 1. The simulations and the exact curve are in excellent agreement, and the ECA prediction does not deviate much for this set.

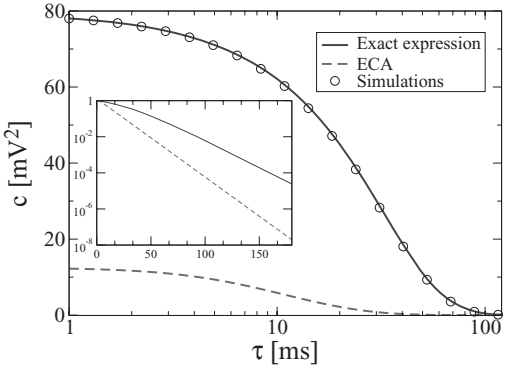

Figure 8: Comparison of the exact autocorrelation function, the ECA prediction, and simulation results for standard set 2. The simulation results and the exact curve are in excellent agreement. In contrast to Figure 7, however, the ECA prediction deviates strongly from the exact result. From the comparison of the normalized curves (inset), it becomes apparent that the timescales also differ.

deviation. Apart from these deviations, there are also strong differences in the timescale (see Figure 8, inset): the ECA predicts a correlation time of $\tau_{c,ECA} = 12$ ms and the exact value is $\tau_{c,ex} = 29$ ms. Here one should keep in mind that the stationary standard deviation does not affect the correlation time.

Apparently the effect of the multiplicative dynamics on the timescale becomes stronger as the shot noise character of the input noise becomes

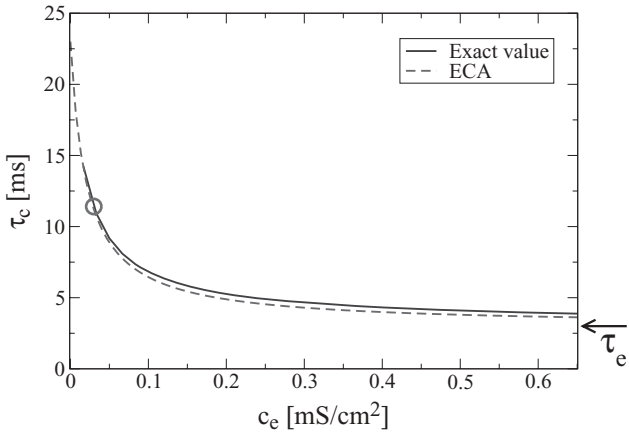

Figure 9: Correlation time versus the parameter c_e for standard set 1. The predictions of the ECA are very close to the exact results. Also for large c_e, the agreement does not become significantly worse. Both curves saturate at τ_e. The point corresponding to the original standard set 1 is indicated by a circle.

stronger, in accordance with the predictions in section 2.3. In the following, we further investigate the dependence of the correlation time on the parameter $c_{e,i}$ and the input rate $r_{e,i}$.

Figure 9 shows an example for the dependence of the correlation time on the parameter c_e. The other parameters are taken from standard set 1. The first observation is that the correlation time decreases with increasing spike amplitude c_e and that the ECA prediction agrees very well with the exact result. The monotonic decrease has been checked for $0.03 \leq c_e \leq 8.3$ (not all data are shown, for clarity).

In Figure 10, the correlation time is plotted versus the parameter c_i for the standard set 2. In this case, there are strong qualitative and quantitative deviations from the prediction of the ECA. Note that there is a distinguished value of c_i, where the correlation time has a minimum, in contrast to the monotonic behavior of the previous example (see Figure 9).

Figures 11 and 12 show the dependence of the correlation time on the synaptic input rate for two different values of the parameter $c_{e,i}$. For moderate $c_{e,i}$ (see Figure 11), the ECA prediction fits well the exact curve. For a more pronounced shot noise input, once again the difference between the simplified and the full dynamics becomes apparent (see Figure 12). Interestingly, the difference between both predictions depends nonmonotonically on the rate (inset in Figure 12). This means that at both low and high rates, there may be regimes where the correlation function is well described by the ECA; however, for moderate spike amplitudes, the ECA might fail.

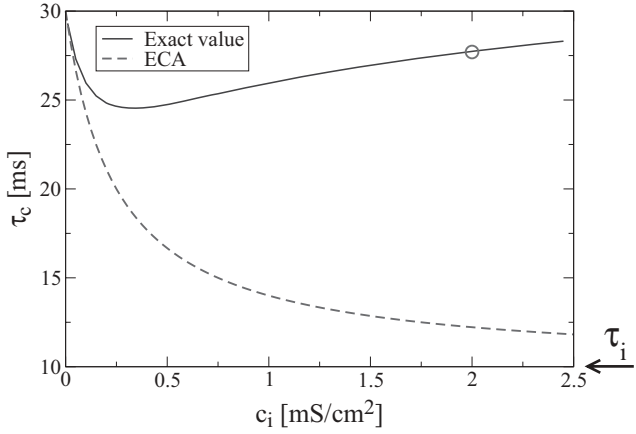

Figure 10: Correlation time in dependence on the spike amplitude c_i for standard set 2. In this example, the agreement of the ECA predictions and the exact values is reasonably good only for very small c_i. Also, the exact correlation times now show a minimum at $c_i \approx 0.3$ mS/cm^2, whereas the ECA predictions decay monotonically. The point corresponding to the original standard set 2 is indicated by a circle.

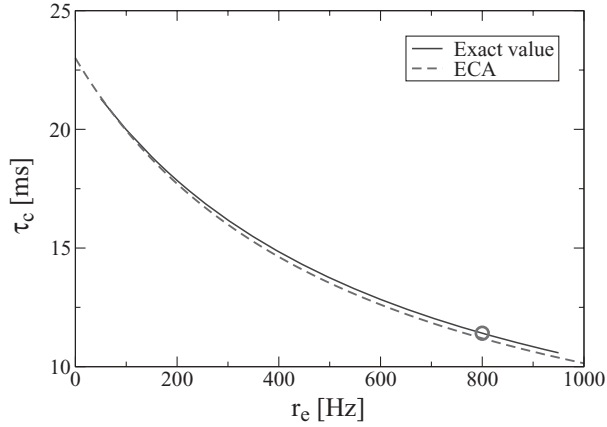

Figure 11: Correlation time in dependence of the input rate for standard set 1. The ECA predictions and the exact values agree well for high as well as for low rates. The original rate of set 1 is indicated by the circle.

4 Discussion

In this letter, we calculated the exact time-dependent mean and variance and the exact stationary autocorrelation function of a passive point neuron

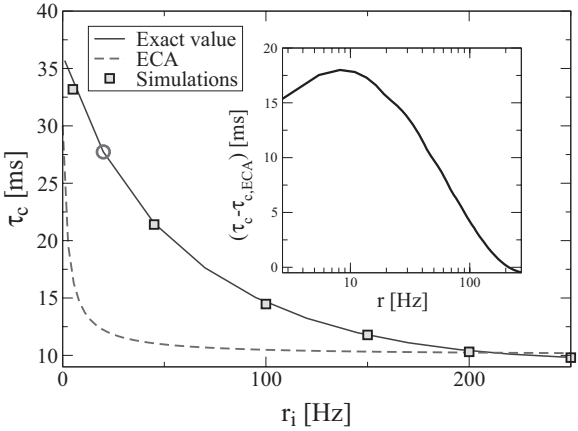

Figure 12: The correlation time in dependence of the input rate for standard set 2. At low rates, strong difference between the exact values and the ECA predictions can be observed. The original rate of set 2 is indicated by the circle.

driven by a filtered conductance shot noise with Poisson statistics. These exact results are rather involved, containing integrals that can only be evaluated numerically. For this reason, we also derived approximations that are based on a small parameter ε that depends on the ratio of spike amplitude and leak conductance and on the ratio of synaptic filter time to membrane time constant. These expressions go beyond the standard approximation (the ECA) and can predict novel effects like extreme values of mean and standard deviation as functions of time. If the parameter $\varepsilon \ll 1$, the approximation predicts the actual time course of mean and standard deviation accurately. However, we also inspected a physiologically plausible parameter set (see Table 2) where $\varepsilon > 1$ and our approximation (not to speak of the ECA) cannot be applied. In such a case, one can only resort to the numerical evaluation of the exact quadrature expressions.

Our results show that for parameters corresponding to many weak input spikes filtered by a fast synapse (see Table 1), the predictions of the ECA for the time-dependent mean value (Figure 3) and for the steady-state value of the standard deviation (asymptotic limit in Figure 5b) are reasonably good, which is in accordance with previous results (Richardson & Gerstner, 2005). Although the nonmonotonic behavior in the mean value is not captured by the ECA, the quantitative deviations of the time-dependent mean value from the ECA predictions will be hard to resolve in this case. However, even for these parameters, the large and measurable transient changes seen in the standard deviation are quantitatively missed in the ECA (cf. the time course in Figure 5) for a broad range of initial voltages. In particular, if we start with a strongly hyperpolarized initial value (see

Figure 5b), the deviation between the true standard deviation and the ECA prediction is off by about 100%. Hyperpolarized initial values are not implausible if we think of the reset mechanism for the voltage-introduced by additional voltage-dependent conductances, for instance, in the Hodgkin-Huxley model.

We demonstrated that the ECA breaks down, as can be expected for larger synaptic weights, lower input rates, and slower synapses. In this case, deviations of the transient and stationary mean value and standard deviation from the predictions of the ECA become a few mV and may thus be easily resolved in experiments.

We also showed that the shot noise character as well as the multiplicative nature of the synaptic noise severely affect the correlation function of the subthreshold voltage (cf. Figure 8). Estimates of the correlation time of voltage, which are based on the ECA, may be off by a factor of two (cf. Figure 12). The correlation time can display a minimum versus the amplitude of the shot noise driving. This is possibly interesting in the context of synaptic plasticity. Neurons undergo short-term and long-term changes in their synaptic efficacies that will lead to a small but nontrivial change in the correlation time of the membrane voltage. The implications of such a change for the neural coding of stimuli are unclear but might be worth exploring.

In conjunction with previous results on the location of the extrema of the mean value (Wolff & Lindner, 2008), our simplified results (see equations 2.20 and 2.22) may be useful to infer parameters of the synaptic input from experiments measuring the time-dependent moments. In particular, the strong maximum seen in the standard deviation may allow a determination of the synaptic timescale or other parameters such as the input rate or the synaptic amplitude $c_{e,i}$. Determining these parameters from the rather shallow minimum in the time-dependent mean voltage requires certainly a very good statistics—many repetitions of clamping and relaxing the voltage. In contrast, the strong maximum in the standard deviation for a hyperpolarized initial voltage may require fewer realizations and may thus be much more practical from the experimental point of view.

A further application of our results is the study of the effect of the conductance shot noise on the spontaneous firing statistics of spiking neurons. An important class of such neuron models comprises those based on a Hazard function (Gerstner & Kistler, 2002), that is, a time-dependent function that gives the probability of the voltage to reach for the first time the firing threshold a given time after the last voltage reset. These models are good approximations to integrate-and-fire models in the subthreshold firing regime driven by a white gaussian current noise (Plesser & Gerstner, 2000) and allow an analytical approximation to the interspike interval (ISI) probability density. Hazard functions involve the time-dependent density of the voltage in the absence of a threshold that can be calculated from the time-dependent mean value (corresponding for a current driving to the

noise-free solution of the voltage equation) and the time-dependent standard deviation. Our result may allow the construction of hazard functions for a subthreshold dynamics driven by a conductance shot noise. In particular, one can use a hazard function that incorporates the time-dependent mean and standard deviation derived in this letter. Note, however, that the incorporation of the third cumulant (giving the skew of the distribution) may turn out to be essential to capture the correct ISI statistics. As shown by Richardson and Gerstner (2005), the skew introduced by both the shot noise character and the multiplicative nature of the conductance noise may be considerable. In principle, one can calculate the third time-dependent cumulant using the method introduced in Wolff and Lindner (2008) and applied here, although this calculation will be rather tedious. As a simple approximation, one may use in the hazard function the steady-state value of the third cumulant, which was derived in Richardson and Gerstner (2005).

From our point of view, an experimental verification of our predictions is highly desirable, in particular, those regarding the nonmonotonic behavior of the mean and standard deviation. To the best of our knowledge, so far no measurements on the time-dependent subthreshold moments have been performed. We hope that this letter will encourage experimental groups to tackle this challenge, as many unexpected effects may be discovered.

Appendix A: Auxiliary Functions

In this appendix, the functions that we abbreviated for simplicity in the main part are given explicitly. For the methods used to calculate these functions, we refer to Wolff and Lindner (2008). For details of the calculations, see Wolff (2007). We use the symbol γ to represent the Euler-Mascheroni constant, $\gamma \approx 0.577$.

The function $f_{e,i}(t)$ for the mean value is given by

$$f_{e,i}(t) = \tau_{\mathrm{e,i}} r_{e,i} (\mathcal{E}i[\varepsilon_{e,i}(e^{-t/\tau_{\mathrm{e,i}}} - 1)] + (\mathcal{E}i[\varepsilon_{e,i}] - \mathcal{E}i[\varepsilon_{e,i} e^{-t/\tau_{\mathrm{e,i}}}]) e^{-\varepsilon_{e,i}} - \ln[\varepsilon_{e,i}(e^{t/\tau_{\mathrm{e,i}}} - 1)] - \gamma). \tag{A.1}$$

For the function $f_{e,i;>}(s, s')$ for the variance, we obtain

$$\begin{aligned} f_{e,i;>}(s, s') = r_{e,i}\tau_{\mathrm{e,i}} \Big(& \mathcal{E}i\left[\varepsilon_{e,i}\left(2e^{\frac{-s}{\tau_{\mathrm{e,i}}}} - e^{\frac{-s}{\tau_{\mathrm{e,i}}}} e^{\frac{s'}{\tau_{\mathrm{e,i}}}} - 1\right)\right] \\ & + e^{-\varepsilon_{e,i}} \mathcal{E}i\left[\varepsilon_{e,i}\left(2e^{\frac{-s'}{\tau_{\mathrm{e,i}}}} - 1\right)\right] - e^{-2\varepsilon_{e,i}} \mathcal{E}i\left[2\varepsilon_{e,i} e^{\frac{-s'}{\tau_{\mathrm{e,i}}}}\right] \\ & - e^{-\varepsilon_{e,i}} \mathcal{E}i\left[\varepsilon_{e,i}\left(2e^{\frac{-s}{\tau_{\mathrm{e,i}}}} - e^{\frac{-s}{\tau_{\mathrm{e,i}}}} e^{\frac{s'}{\tau_{\mathrm{e,i}}}}\right)\right] + e^{-2\varepsilon_{e,i}} \mathcal{E}i[2\varepsilon_{e,i}] \\ & - \ln\left(\varepsilon_{e,i}\left(e^{\frac{s}{\tau_{\mathrm{e,i}}}} + e^{\frac{s'}{\tau_{\mathrm{e,i}}}} - 2\right)\right) - \gamma \Big). \end{aligned} \tag{A.2}$$

Finally, the functions $f^{+}_{e,i>}(\tau, s, s')$ and $f^{-}_{e,i>}(\tau, s, s')$ read

$$\begin{aligned}
&f^{+}_{e,i>}(\tau, s, s') \\
&= r_{e,i}\tau_{\mathrm{e,i}}\Big(e^{-\varepsilon_{e,i}}\mathcal{E}i[\varepsilon_{e,i}] + \mathcal{E}i\Big[\varepsilon_{e,i}\Big(e^{-\frac{s}{\tau_{\mathrm{e,i}}}} + e^{-\frac{s+\tau}{\tau_{\mathrm{e,i}}}} - e^{-\frac{s-s'}{\tau_{\mathrm{e,i}}}} - 1\Big)\Big] \\
&\quad + e^{-\varepsilon_{e,i}}\mathcal{E}i\Big[\varepsilon_{e,i}\Big(e^{-\frac{s'}{\tau_{\mathrm{e,i}}}} + e^{-\frac{s'+\tau}{\tau_{\mathrm{e,i}}}} - 1\Big)\Big] - e^{-\varepsilon_{e,i}}\mathcal{E}i\Big[\varepsilon_{e,i}e^{-\frac{\tau}{\tau_{\mathrm{e,i}}}}\Big] \\
&\quad - e^{-\varepsilon_{e,i}}\mathcal{E}i\Big[\varepsilon_{e,i}\Big(e^{-\frac{s}{\tau_{\mathrm{e,i}}}} + e^{-\frac{s+\tau}{\tau_{\mathrm{e,i}}}} - e^{-\frac{s-s'}{\tau_{\mathrm{e,i}}}}\Big)\Big] - \frac{s+\tau}{\tau_{\mathrm{e,i}}} \\
&\quad - e^{-2\varepsilon_{e,i}}\mathcal{E}i\Big[\varepsilon_{e,i}\Big(e^{-\frac{s'}{\tau_{\mathrm{e,i}}}} + e^{-\frac{s'+\tau}{\tau_{\mathrm{e,i}}}}\Big)\Big] + e^{-2\varepsilon_{e,i}}\mathcal{E}i\Big[\varepsilon_{e,i}\Big(e^{-\frac{\tau}{\tau_{\mathrm{e,i}}}} + 1\Big)\Big] \\
&\quad - \ln\Big[\varepsilon_{e,i}\Big(1 + e^{-\frac{s-s'}{\tau_{\mathrm{e,i}}}} - e^{-\frac{s+\tau}{\tau_{\mathrm{e,i}}}} - e^{-\frac{s}{\tau_{\mathrm{e,i}}}}\Big)\Big] - \gamma\Big)
\end{aligned} \tag{A.3}$$

and

$$\begin{aligned}
&f^{-}_{e,i>}(\tau, s, s') \\
&= r_{e,i}\tau_{\mathrm{e,i}}\Big(-e^{-\varepsilon_{e,i}}\mathcal{E}i\Big[\varepsilon_{e,i}e^{-\frac{s'+\tau}{\tau_{\mathrm{e,i}}}}\Big] + \mathcal{E}i\Big[\varepsilon_{e,i}\Big(e^{-\frac{s'+\tau}{\tau_{\mathrm{e,i}}}} - 1\Big)\Big] \\
&\quad + \mathcal{E}i\Big[\varepsilon_{e,i}\Big(e^{-\frac{s}{\tau_{\mathrm{e,i}}}} + e^{-\frac{s+\tau}{\tau_{\mathrm{e,i}}}} - e^{-\frac{s-s'}{\tau_{\mathrm{e,i}}}} - 1\Big)\Big] - \frac{\tau}{\tau_{\mathrm{e,i}}} \\
&\quad + e^{-\varepsilon_{e,i}}\mathcal{E}i\Big[\varepsilon_{e,i}\Big(1 - e^{\frac{s'}{\tau_{\mathrm{e,i}}}} + e^{-\frac{\tau}{\tau_{\mathrm{e,i}}}}\Big)\Big] - \mathcal{E}i\Big[\varepsilon_{e,i}\Big(e^{-\frac{\tau}{\tau_{\mathrm{e,i}}}} - e^{\frac{s'}{\tau_{\mathrm{e,i}}}}\Big)\Big] \\
&\quad - e^{-\varepsilon_{e,i}}\mathcal{E}i\Big[\varepsilon_{e,i}\Big(e^{-\frac{s}{\tau_{\mathrm{e,i}}}} + e^{-\frac{s+\tau}{\tau_{\mathrm{e,i}}}} - e^{-\frac{s-s'}{\tau_{\mathrm{e,i}}}}\Big)\Big] + e^{-\varepsilon_{e,i}}\mathcal{E}i[\varepsilon_{e,i}] \\
&\quad - \ln\Big[\varepsilon_{e,i}\Big(e^{\frac{s}{\tau_{\mathrm{e,i}}}} + e^{\frac{s'}{\tau_{\mathrm{e,i}}}} - e^{-\frac{\tau}{\tau_{\mathrm{e,i}}}} - 1\Big)\Big] - \gamma\Big),
\end{aligned} \tag{A.4}$$

respectively.

Appendix B: Coefficients for the Systematic Approximation

In the following, the subscripts e, i will be omitted.

B.1 Coefficients for the Mean Value. The coefficients for the mean value read:

$$c_{\langle v\rangle,1}(t) = (v_0 - v_e r\varepsilon\tau_0)\left(1 + \frac{r\varepsilon^2}{2}(t-\tau)\right) + \frac{r\varepsilon^2}{2}v_e\tau_0^2\beta \tag{B.1}$$

and

$$c_{\langle v\rangle,2} = \frac{r\varepsilon^2}{2}\tau\left(v_0 - v_e\frac{1+r\tau\varepsilon}{(1+\tau/\tau_0)}\right). \tag{B.2}$$

B.2 Coefficients for the Second Moment. To derive the approximate expression for the second moment, we use the following expansion:

$$\exp[f(s,s')] \approx e^{-r\varepsilon(s+s')}\Bigg(1 + r\tau\varepsilon^2\Bigg(e^{-s'/\tau} + e^{-s/\tau} - \frac{1}{2}\exp\left[-\frac{s-s'}{\tau}\right] + \frac{1}{2}\left(\frac{s}{\tau} + 3\frac{s'}{\tau} - 3\right)\Bigg)\Bigg). \tag{B.3}$$

The coefficients read:

$$\begin{aligned} c_{\langle v^2\rangle,1} = {} & v_0^2 + \frac{r\varepsilon\tau_0}{\tau-\tau_0}\Bigg[-2v_0v_e(\tau-\tau_0) \\ & + \varepsilon v_e\left(\frac{v_e\tau_0}{2}(1+2r(\tau-\tau_0)) + v_0(2\tau-3\tau_0) - 2\frac{v_0^2}{v_e}\frac{\tau}{\tau_0}(\tau-\tau_0)\right) \\ & + 2r\varepsilon^2 v_0\left(\tau_0^2\left(v_e + \frac{3}{2}v_0\right) - \tau_0\tau(v_e+3v_0) + 2v_0\tau^2\right) \\ & + \frac{r^2\varepsilon^3 v_e^2\tau_0}{2}\left(8\tau_0\tau - 4\tau^2 - 5\tau_0^2\right)\Bigg] \\ & + \left[2r^3\varepsilon^4\tau_0^2v_e^2 - 4r^2\varepsilon^3v_0v_e\tau_0 + 2r\varepsilon^2v_0^2\right]t, \end{aligned} \tag{B.4}$$

$$\begin{aligned} c_{\langle v^2\rangle,2} = {} & \frac{r\varepsilon v_e\tau_0}{\tau+\tau_0}\big[2v_0(\tau+\tau_0) - \varepsilon(2\tau_0 r v_e(\tau+\tau_0) + v_0(3\tau_0+\tau)) \\ & + r\varepsilon^2\left(2v_e\left(\tau_0\tau + 2\tau_0^2\right) + v_0\left(3\tau_0^2 - \tau^2\right)\right) + r^2\varepsilon^3 v_e\tau_0\left(\tau^2 - \tau_0\tau - 4\tau_0^2\right)\big] \\ & + \left[r^2\varepsilon^3v_0v_e\tau_0 - r^3\varepsilon^4\tau_0^2v_e^2\right]t, \end{aligned} \tag{B.5}$$

$$\begin{aligned} c_{\langle v^2\rangle,3} = {} & \frac{2r\varepsilon^2\tau}{\tau+\tau_0}\big[v_0\left(v_0\tau + \tau_0(v_0-v_e)\right) \\ & + r\varepsilon v_e\tau_0\left(\tau_0(v_e-v_0) - 2v_0\tau\right) + r^2\varepsilon^2v_e^2\tau\tau_0^2\big], \end{aligned} \tag{B.6}$$

$$\begin{aligned} c_{\langle v^2\rangle,4} = {} & \frac{r v_e\tau_0\tau\varepsilon^2}{\tau^2-\tau_0^2}\big[(v_0-v_e)\tau + v_0\tau_0 - r\varepsilon\left(2v_e\tau_0\left(\tau-\tau_0\right)\right. \\ & \left. + v_0\left(\tau_0^2 - \tau\tau_0 - 3\tau^2\right)\right) + r^2\varepsilon^2v_e\tau\tau_0(2\tau_0-\tau)\big], \end{aligned} \tag{B.7}$$

and

$$c_{\langle v^2\rangle,5} = \frac{r v_e^2 \tau_0^2 \varepsilon^2}{\tau + \tau_0} \left[1 + 2r(\tau + \tau_0) - 2r\tau_0\varepsilon + \frac{3}{2} r^2 \tau_0^2 \varepsilon^2 \right]. \tag{B.8}$$

References

Brunel, N., & Sergi, S. (1998). Firing frequency of leaky integrate-and-fire neurons with synaptic current dynamics. *J. Theor. Biol.*, *195*, 87–95.

Burkitt, A. N. (2001). Balanced neurons: Analysis of leaky integrate-and-fire neurons with reversal potentials. *Biol. Cybern.*, *85*, 247–255.

Burkitt, A. N. (2006). A review of the integrate-and-fire neuron model: I. Homogeneous synaptic input. *Biol. Cybern.*, *95*, 1.

Destexhe, A., & Mainen, Z. F. (1994). Synthesis of models for excitable membranes, synaptic transmission and neuromodulation using a common kinetic formalism. *J. Comput. Neurosci.*, *1*, 105–230.

Gardiner, C. W. (1985). *Handbook of stochastic methods*. Berlin: Springer-Verlag.

Gerstner, W., & Kistler, W. M. (2002). *Spiking neuron models*. Cambridge: Cambridge University Press.

Hanson, F. B., & Tuckwell, H. C. (1983). Diffusion approximation for neuronal activity including synaptic reversal potentials. *J. Theor. Neurobiol.*, *2*, 127–153.

Holden, A. V. (1976). *Models of the stochastic activity of neurones*. Berlin: Springer-Verlag.

Johannesma, P. (1968). Diffusion models of the stochastic activity of neurons. In E. Caianiello (Ed.), *Neural networks* (pp. 116–144). Berlin: Springer.

Koch, C. (1999). *Biophysics of computation: Information processing in single neurons*. New York: Oxford University Press.

Lánský, P., & Lánská, V. (1987). Diffusion approximation of the neuronal model with synaptic reversal potentials. *Biol. Cybern.*, *56*, 19–26.

Lindner, B., & Longtin, A. (2006). Comment on "Characterization of sub-threshold voltage fluctuations in neural membranes" by M. Rudolph and A. Destexhe. *Neural Comput.*, *18*(8), 1896–1931.

Plesser, H. E., & Gerstner, W. (2000). Escape rate models for noisy integrate-and-fire neurons. *Neurocomputing*, *32–33*, 219.

Ricciardi, L. M. (1977). *Diffusion processes and related topics on biology*. Berlin: Springer-Verlag.

Richardson, M. J. E. (2004). Effects of synaptic conductance on the voltage distribution and firing rate of spiking neurons. *Phys. Rev. E*, *69*, 051918.

Richardson, M., & Gerstner, W. (2005). Synaptic shot noise and conductance fluctuations affect the membrane voltage with equal significance. *Neural Comput.*, *17*(4), 923–947.

Rudolph, M., Piwkowska, Z., Badoual, M., Bal, T., & Destexhe, A. (2004). A method to estimate synaptic conductances from membrane potential fluctuations. *J. Neurophysiol.*, *91*, 2884–2896.

Stein, R. B. (1965). A theoretical analysis of neuronal variability. *Biophys. J.*, *5*, 173–194.

Stein, R. B. (1967). Some models of neuronal variability. *Biophys. J.*, *7*(1), 37–68.

Tuckwell, H. C. (1979). Synaptic transmission in a model for stochastic neural activity. *J. Theor. Biol.*, *77*, 65–81.

Tuckwell, H. C. (1989). *Stochastic processes in the neurosciences*. Philadelphia: SIAM.

Wolff, L. (2007). *Sub-threshold fluctuations of a conductance based point neuron under the influence of synaptic shot noise*. Unpublished master's thesis, Technische Universität Dresden, Germany.

Wolff, L., & Lindner, B. (2008). A method to calculate the moments of the membrane voltage in a model neuron driven by multiplicative filtered shot noise. *Phys. Rev. E*, *77*, 041913.

Received February 9, 2009; accepted May 4, 2009.